Journal of Physics: Condensed Matter

PAPER • **OPEN ACCESS**

In situ synchrotron XRD measurements during solidification of a melt in the CaO–SiO_2 system using an aerodynamic levitation system

To cite this article: Katharina Schraut *et al* 2021 *J. Phys.: Condens. Matter* **33** 264003

OPEN ACCESS
IOP Publishing
Journal of Physics: Condensed Matter
J. Phys.: Condens. Matter **33** (2021) 264003 (12pp)
https://doi.org/10.1088/1361-648X/abf7e1

In situ synchrotron XRD measurements during solidification of a melt in the $CaO–SiO_2$ system using an aerodynamic levitation system

Katharina Schraut[1,*], Florian Kargl[2], Christian Adam[1] and Oleh Ivashko[3]

[1] Division Thermochemical Residues Treatment and Resource Recovery, Bundesanstalt für Materialforschung und -prüfung (BAM), Unter den Eichen 87, 12205 Berlin, Germany
[2] Institut für Materialphysik im Weltraum, Deutsches Zentrum für Luft und Raumfahrt (DLR), Linder Höhe, 51170 Köln, Germany
[3] Deutsches Elektronen-Synchrotron DESY, Notkestraße 85, 22607 Hamburg, Germany

E-mail: katharina.schraut@bam.de

Received 5 February 2021, revised 22 March 2021
Accepted for publication 14 April 2021
Published 26 May 2021

Abstract

Phase formation and evolution was investigated in the $CaO–SiO_2$ system in the range of 70–80 mol% CaO. The samples were container-less processed in an aerodynamic levitation system and crystallization was followed *in situ* by synchrotron x-ray diffraction at the beamline P21.1 at the German electron synchrotron (DESY). Modification changes of di- and tricalcium silicate were observed and occurred at lower temperatures than under equilibrium conditions. Despite deep sample undercooling, no metastable phase formation was observed within the measurement timescale of 1 s. For the given cooling rates ranging from 300 K s^{-1} to about 1 K s^{-1}, no decomposition of tricalcium silicate was observed. No differences in phase evolution were observed between reducing and oxidizing conditions imposed by the levitation gas (Ar and Ar + O_2). We demonstrate that this setup has great potential to follow crystallization in refractory oxide liquids *in situ*. For sub-second primary phase formation faster detection and for polymorph detection adjustments in resolution have to be implemented.

Keywords: aerodynamic levitation, calcium silicate, phase formation, oxide melts, *In situ* synchrotron x-ray diffraction

(Some figures may appear in colour only in the online journal)

1. Introduction

At the time when the first equilibrium phase diagrams were generated for the system $CaO–SiO_2$, the existence, the stability and the formation of tricalcium silicate were controversially discussed (Day and Shepherd 1906, Rankin 1915, Kühl 1951). Some years later, the melting point of tricalcium silicate was determined by Nurse (1960) to be 2070 °C.

Tricalcium silicate is a nesosilicate consisting of isolated SiO_4 tetrahedrons and oxygen ions octahedrally coordinated by Ca^{2+} ions (Ludwig and Zhang 2015). Seven modifications of tricalcium silicate were identified between room temperature and the melting point by differential thermal analysis (DTA), high temperature x-ray diffraction (XRD) and high-temperature optical microscopy (Stephan 1999). Between the melting point and 1070 °C pure tricalcium silicate is trigonal

* Author to whom any correspondence should be addressed.

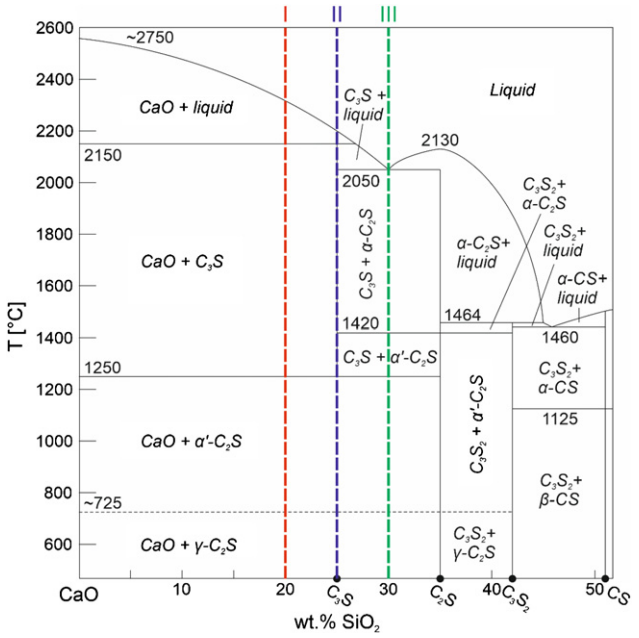

Figure 1. Section of the equilibrium phase diagram CaO–SiO_2 from 0 to 55 wt.% SiO_2 (modified after Macphee and Lachowski (2003)). The compositions of the investigated mixtures I–III are marked. Abbreviations for mineral formulas: C = CaO, S = SiO_2. Reprinted from Macphee and Lachowski (2003), Copyright (2003), with permission from Elsevier.

(space group $R3m$). During continuous cooling, the symmetry of tricalcium silicate gradually decreases and its unit cell volume increases (Bigare *et al* 1967, Bazzoni *et al* 2014). Between 980–1070 °C three monoclinic modifications (space group $C1m1$) occur: 1060–1070 °C M3; 990–1060 °C M2, 980–990 °C M1, and between room temperature and 980 °C three triclinic modifications (T1 and T3 space group $P\bar{1}$, T2 space group disputed) occur: 920–980 °C T3, 620–920 °C T2, <620 °C T1 (De La Torre *et al* 2002, Dunstetter *et al* 2006, De Noirfontaine *et al* 2012, Bazzoni *et al* 2014). All modifications changes are displacive (Bigare *et al* 1967) and have low transformation enthalpies (Dunstetter *et al* 2006). The unit cells of the monoclinic and triclinic polymorphs result from minute distortion of the rhombohedral unit cell by an orientation change of the SiO_4 tetrahedra (Bigare *et al* 1967, Bazzoni *et al* 2014).

The polymorphs can be distinguished in the angular ranges 32 to 33 °$2\theta_{Cu}$ and 51 to 52 °$2\theta_{Cu}$ by characteristic subcell reflections (Sinclair and Groves 1984). During cooling, the $\bar{2}04$ reflection of the trigonal cell at 32 to 33 °$2\theta_{Cu}$ splits into the two $2\bar{2}4$ and $\bar{4}04$ reflections of the monoclinic cell and during further cooling into the three reflections of the triclinic cell 224, $2\bar{2}4$ and $\bar{4}04$ (Yamaguchi and Miyabe 1960). Similarly, one can observe this change at 51–52 °$2\theta_{Cu}$ were 220 reflection of the trigonal cell splits into the 040 and 620 reflections of the monoclinic cell and later in the 040, 620 and $\bar{6}20$ reflections of the triclinic cell (Yamaguchi and Miyabe 1960).

The gradual modification changes only occur as long as no foreign ions are incorporated into the tricalcium silicate structure and stabilize a high-temperature polymorph (Bazzoni *et al* 2014). The solid solution of tricalcium silicate with foreign ions such as Al^{3+}, Mg^{2+} and Fe^{2+}/Fe^{3+} is termed alite and is the most important mineral in ordinary Portland cement (OPC). Alite occurs mostly in the M1 and M3 modification (Maki *et al* 1991).

Table 1. Chemical composition of the annealed mixtures I–III determined by ICP-OES after total digestion (HNO_3/$HClO_4$/HF). The error indicates the simple standard deviation of three replicate measurements of each two samples per mixture ($N = 6$).

	Mixture I	Mixture II	Mixture III
CaO [wt.%]	79 ± 3	75 ± 5	68 ± 4
SiO_2 [wt.%]	22.2 ± 0.3	24.8 ± 0.3	29.9 ± 0.8

In thermodynamic equilibrium, pure tricalcium silicate is stable above 1250 ± 25 °C (figure 1) (Lea and Parker 1934, Mohan and Glasser 1977). Below this temperature tricalcium silicate decomposes to dicalcium silicate and CaO. Hereby, the rate of decomposition is temperature dependent. Decomposition is highest between 1025–1175 °C (Carlson 1931, Mohan and Glasser 1977, Li *et al* 2014) and becomes imperceptible below 700 °C (Taylor 1997). Moreover, the presence of the decomposition products dicalcium silicate and CaO strongly affects the decomposition rate (Mohan and Glasser 1977).

Tricalcium silicate undergoes the phase transformations described above in a metastable state. The decomposition rate is low enough that the metastable mineral changes its modification during cooling without decaying as long as thermodynamic equilibrium is not reached. On the whole, the decomposition of tricalcium silicate is so slow that complete decomposition rarely occurs (Lea and Parker 1934). In laboratory studies, it takes several days before signs of the decomposition of tricalcium silicate can be observed (Woermann 1960). Investigations by Glasser (1998) showed that a complete decomposition of tricalcium silicate at 1175 °C requires about 600 h.

It should be noted, however, that in contrast to the observations under laboratory conditions, the decomposition of alite in technical cement production has been repeatedly observed and attributed to too slow cooling in the critical temperature zone (Woermann 1960).

Another major constituent of OPC is belite, the solid solution of the stabilized β-modification of dicalcium silicate. Dicalcium silicate is also a nesosilicate and undergoes in pure form four modification changes between melt and room temperature. Between the melting point of 2150 °C (Chan *et al* 1992) and 1425 °C the hexagonal α-modification ($P6_3/mmc$) is stable. Between 1425–1177 °C the orthorhombic α'_H-modification ($Pnma$) and between 850–1177 °C the orthorhombic α'_L-modification ($Pna2_1$) occurs (Chan *et al* 1992). α'_L transforms either directly to the orthorhombic γ-modification ($Pna2_1$), which is stable at room temperature, or to the monoclinic β-modification ($P12_1/n1$), which is stable between 490–675 °C (Chan *et al* 1992). The transformation from β- to γ-modification at 490 °C is characterized by a 4.6° angular unit-cell change due to rotation of the SiO_4 tetrahedra and movements of Ca^{2+} ions, resulting in a significant volume increase of 12% (Ghosh *et al* 1979, Chan *et al* 1992, Durinck

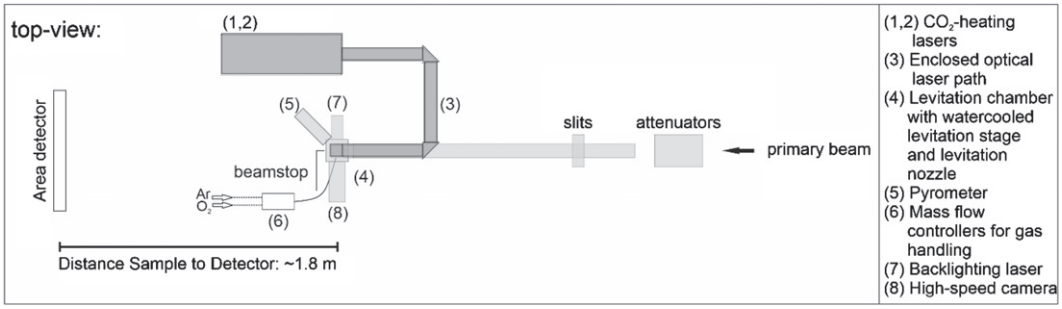

Figure 2. Sketch of the ADL setup at beamline P21.1 at DESY. The sketch shows a top view on to the x–y–z stage. Sample installation is carried out via the beam-exit window to the levitation chamber. To this end the beamstop is moved to its end-position to provide free-access to the levitation chamber and nozzle onto which the sample is mounted.

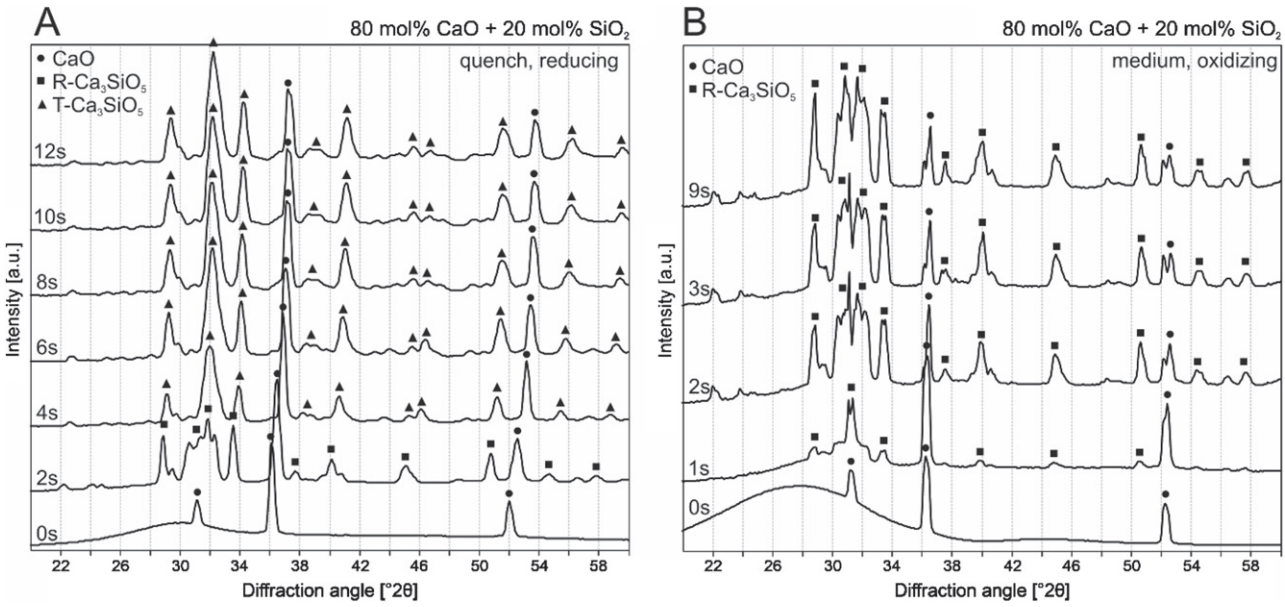

Figure 3. Detail of x-ray diffractograms (20–60 °$2\theta_{Cu}$) of samples from mixture I. (A) Diffractograms from the first 12 s after quenching under reducing conditions. (B) Diffractograms from the first 9 s medium cooling under oxidizing conditions. The time point 0 was set to the last diffraction pattern before Ca_3SiO_5 crystallization.

et al 2008). The β-modification can be stabilized at room temperature by critical size ratio for individual particles (Chan *et al* 1992), by rapid cooling (Durinck *et al* 2008) or incorporation of foreign ions such as B^{3+}, Na^{+}, K^{+}, Ba^{2+}, Mn^{2+}/Mn^{3+} or Cr^{3+} (Ghosh *et al* 1979).

The formation of alite and belite via the solid-state processes during Portland cement burning in the rotary kiln is well investigated and understood. The crystallization of calcium silicates from the melt, on the other hand, is less well studied. This is not least connected with the difficulties of experimental studies including *in situ* structure analysis at temperatures above 2000 °C.

The modification changes of tricalcium silicate as a function of temperature have mostly been studied with DTA and high-temperature optical microscopy. In contrast, the diffraction methods required for structure solutions, such as the Weissenberg method (Jeffery 1952, Golovastikov *et al* 1975), synchrotron x-ray powder diffraction and neutron powder diffraction (De La Torre *et al* 2002), only allow direct analysis of the triclinic polymorph of pure tricalcium silicate, as the others are not stable at room temperature. Therefore, alites containing Mg^{2+} and Al^{3+} (M3 polymorph) (Jeffery 1952, De La Torre *et al* 2002, De Noirfontaine *et al* 2012) or Al^{3+}, Mg^{2+}, Fe^{2+}/Fe^{3+} and S^{6+} (M1 polymorph) (De Noirfontaine *et al* 2012) were mostly used for structure solution of the monoclinic polymorphs of tricalcium silicate.

A direct investigation of pure tricalcium silicate at temperatures up to 1100 °C was performed by Yannaquis *et al* (1962) using a special heating chamber and Debye–Scherrer diffraction. Other studies which investigated calcium silicates (Benmore *et al* 2010) have focused on the melt phase and glass formation rather than *in situ* observation of phase evolution during crystallization.

To reach temperatures beyond the melting point, aerodynamic levitation (ADL) was used and coupled with synchrotron XRD. ADL avoids common problems with crucible materials such as reaction with and contamination by the crucible and suppresses heterogeneous nucleation. Due to processing on a gas stream, the conditions can be set from reducing to oxidizing by varying gas composition. Cooling

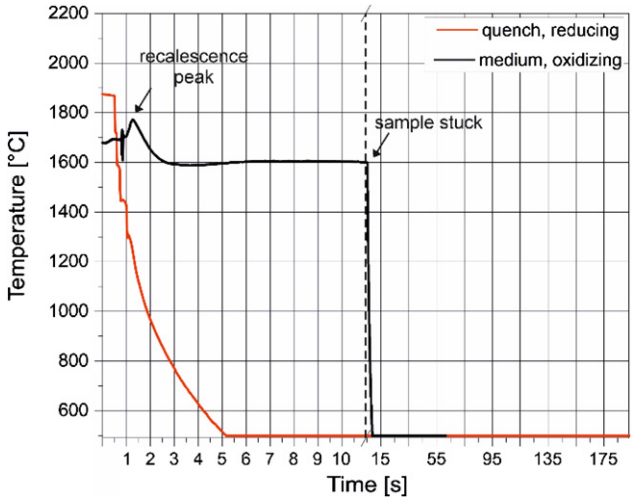

Figure 4. Temperature curves of samples from mixture I during cooling measured with a pyrometer. The time point 0 was set to 1 s before crystallization of Ca_3SiO_5.

rates can be easily varied in a wide range (100s of degree per second to few degrees per minute). In the present work, a combination of ADL and synchrotron XRD was used to explore different crystallization scenarios. The ADL was equipped with two high-power lasers that allowed sample temperatures up to 2380 °C.

2. Materials and methods

2.1. Sample preparation

Three mixtures composed of (I) 80 mol% CaO + 20 mol% SiO_2, (II) 75 mol% CaO + 25 mol% SiO_2 and (III) 70 mol% CaO + 30 mol% SiO_2 were prepared using $CaCO_3$ from abcr GmbH (99.95–100.05 %) and SiO_2 from J.T. Baker (p.a.). The chemical composition of mixture II corresponds to the chemical composition of alite as the main mineral phase in Portland cement clinker and is thus of particular interest. Mixtures I and III differ from mixture II in 5 mol% higher and lower CaO content and enable the investigation of variation in chemical composition and differing crystallization paths.

The mixtures were homogenised in a mixer-mill from SPEX SamplePrep for 10 min. The homogenised mixtures were decarbonated by annealing the mixtures for 1 h at 1000 °C in a chamber furnace. The annealing procedure was repeated three times. Between the annealing steps, the mixtures were ground in a mortar.

Several pressed powder tablets of about 1 cm in diameter and approximately 200 mg weight were produced from the decarbonated mixtures with a Perkin–Elmer hydraulic press at a pressure of 10 T under vacuum. The pressed tablets were annealed for 12 h at 1450°C in air. The annealed tablets were ground in a mortar and pressed and annealed again. After the second annealing, solid tablets were obtained for mixtures I and II. The tablets of mixture III could not be stabilized by annealing and disintegrated to powder. This can be attributed to the solid-state transition of β- to γ-Ca_2SiO_4, which is accompanied by a significant volume increase and causes the tablets to decompose (Chan *et al* 1992). Therefore, powder tablets were pressed from fourfold annealed material from mixture III.

The chemical composition of the annealed mixtures was validated by inductively coupled plasma optical emission spectrometry (ICP-OES) using an iCAP 6500 Fisher Scientific (table 1). For this purpose, the 0.1 g of the mixtures were digested with a total digestion (HNO_3/$HClO_4$/HF) in a microwave. All mixtures were measured as duplicates.

For the levitation experiments spherical samples with approximately 2 mm diameter are required. Therefore, small pieces of 10 to 15 mg were broken from the prepared tablets and melted in the same ADL used for the synchrotron experiments in a special production nozzle with a high rim. The production time lasted between several seconds to about 1–2 min sometimes in combination with several heating and cooling cycles. It was not possible to prepare spheres from mixture III because the samples disintegrated during cooling to a fine powder as expected from the literature (Chan *et al* 1992). Interestingly, a fast quench of the liquid led to immediate formation of fine powder when the β to γ transition range was reached whereas a slower cooling led to a slightly delayed disintegration. This behaviour has to be explored in more detail since it is not directly conforming to the behaviour reported by Chan *et al* (1992). Mixtures III therefore had to be melted directly from the tablet fragment in the ADL installed at the synchrotron in the low-rimmed high-sample-visibility nozzle.

Spheres of mixture I were also difficult to prepare due to the high melting point of the mixture. Only partially molten samples could be prepared before the experiment. For mixture I, non-stoichiometric evaporation is a challenge, restricting the measurement to a short period of time. With longer processing times, the sample eventually becomes fully liquid due to CaO-loss.

2.2. Experimental setup

The samples were container-less processed in an ADL system. The system is described in detail by Kargl *et al* (2015). The ADL was adapted for its first-time use at DESY. The high-speed camera position was changed by 90° and was used for monitoring of the sample. A second small camera was implemented at the top of the levitation chamber providing an angled top-view to the levitated sample for process control. In addition, the original single-color pyrometer operating at a wavelength close to 1 μm was exchanged for a single-color pyrometer operating at a wavelength of 5.14 μm (IMPAC IN140/5-L MB25). This conforms better to the emission characteristics of silicate melts, which show a constant and high emissivity at this wavelength. To protect the pyrometer optics from evaporated material a sacrificial CaF window was implemented in the beam-path of the pyrometer. The windows transmission of 97 % was taken into account when setting the emissivity value for the pyrometer. The breadboard with the levitation system was directly fixed to the x–y–z stage at beamline P21.1 at PETRA III, DESY. The x-ray beam passed through the original backlight-laser-high-speed camera path. The windows sealing-off the chamber from the surroundings were replaced by two windows conforming to the XRD measurements.

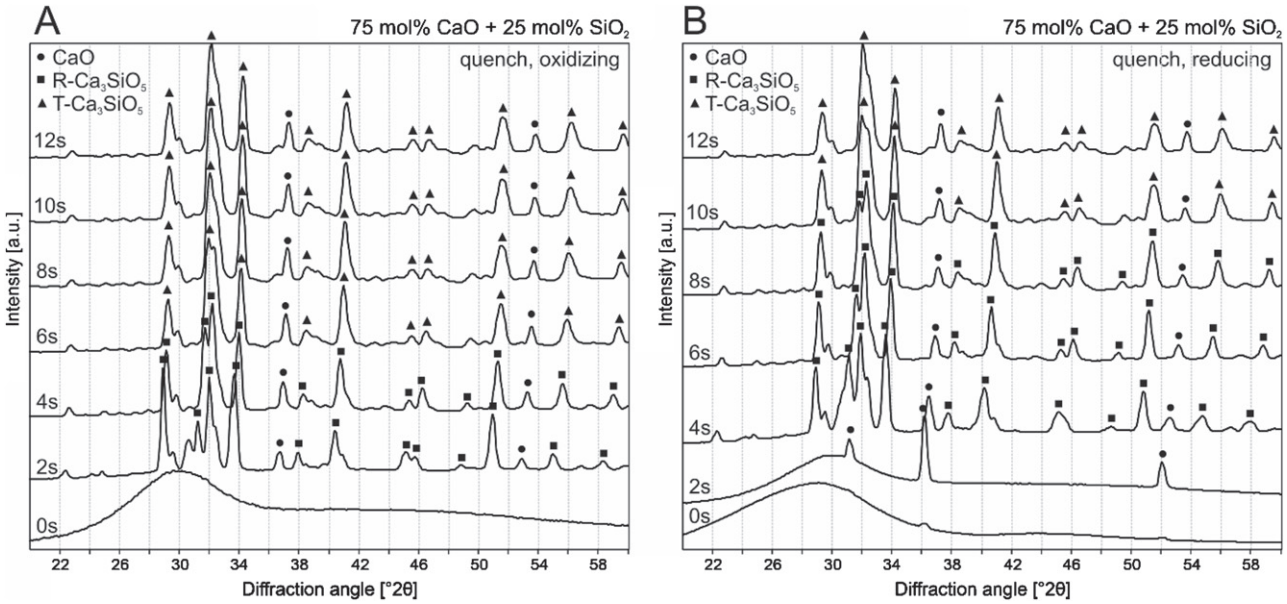

Figure 5. Detail of x-ray diffractograms (20–60 $°2\theta_{Cu}$) of quenched samples from mixture II under (A) oxidizing conditions and (B) reducing conditions. The time point 0 was set to the last diffraction pattern before crystallization.

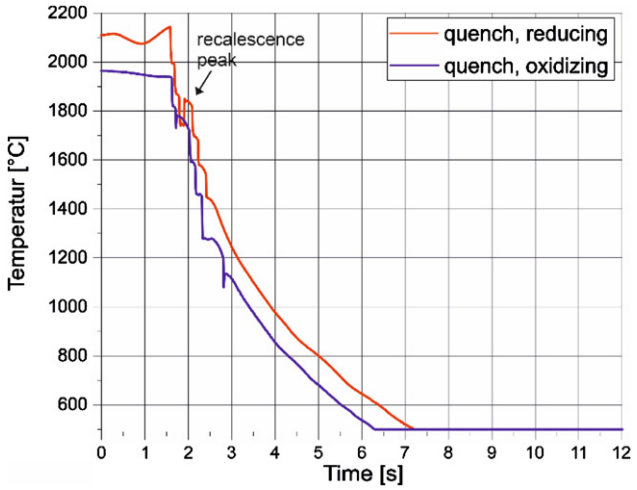

Figure 6. Temperature curves of quenched samples from mixture II measured with a pyrometer. The time point 0 was set to 1 s before crystallization.

On the exit side of the sample chamber, the beam passed a 0.5 mm thin Al-window of approximately 40 mm diameter positioned about 25 mm from the sample before reaching the detector. Bragg peaks caused by scattering of the primary x-ray beam were cut out by positioning the beamstop close to this Al-window. On the entrance side of the chamber the thin Al-window was replaced by a window made of glass due to the strong and non-uniform Bragg-peaks generated on the detector by an initially used equally thin Al-window. The glass window was of course thicker (about 3 mm) and therefore lead to a higher but amorphous background signal. The diameter of the glass window was about 15 mm positioned about 30 mm from the sample. A sketch of the levitation setup at beamline P21.1 is shown in figure 2. The system was connected to the mobile laser-interlock unit provided by DESY to sustain safe operation. For on-site sample production the levitator could be operated in manual mode with one or two operators present in the experiment hutch (no x-ray operation) wearing suitable safety googles as additional pre-caution. When operating the laser in the x-ray beam a remote control of the entire facility from the experiment-control room was possible via wired communication with the control computers.

2.3. Experimental procedure

10 to 15 mg sample pieces were levitated by means of a gas-jet directed through a converging–diverging nozzle. Either spherical samples prepared in the levitator were inserted in the low-rimmed nozzle or irregularly shaped pressed-powder pieces were inserted into this nozzle (mixture III). The freely suspend samples (mixtures I and II) or the irregularly shaped piece with minimal contact (mixture III) were heated by laser-radiation of two CO_2 lasers until the melting point was reached. Heating, especially from below, ensures a homogeneous sample temperature. By using either pure Ar gas or a mixture of Ar and O_2 gas, reducing or oxidizing conditions were generated. Three different cooling rates were used to evaluate the influence of cooling conditions on the crystallization. The laser power was lowered by 0.01 % s^{-1} or 0.08–0.1 % s^{-1}, which resulted in cooling times of 1.5–2 h or 10 min, respectively or was shut down, which resulted in immediate cooling withing 1–2 s (quench). Representative cooling curves are shown in figures 4, 6, 8 and 10.

The levitated molten droplets had a diameter of about 2 mm and were measured with a 0.9 mm x-ray beam centred on the sample. The x-ray beam had a wavelength of 0.122 Å. An x-ray diffractogram was recorded every second on a 2D area detector Varex XRD 4343 CT with an amorphous silicon TFT diode array. The detector had a pixel number of 2880 × 2880 and a pixel size of 150 × 150 μm^2.

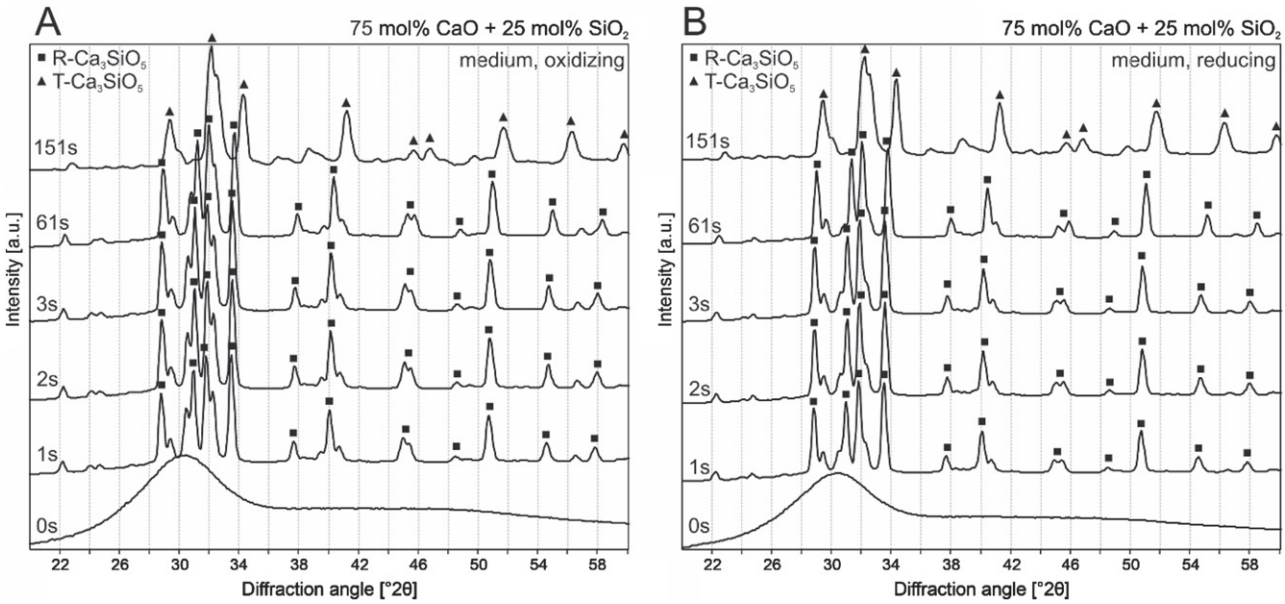

Figure 7. Detail of x-ray diffractograms (20–60 $°2\theta_{Cu}$) of medium cooled samples from mixture II under (A) oxidizing conditions and (B) reducing conditions. The time point 0 was set to the last diffraction pattern before crystallization.

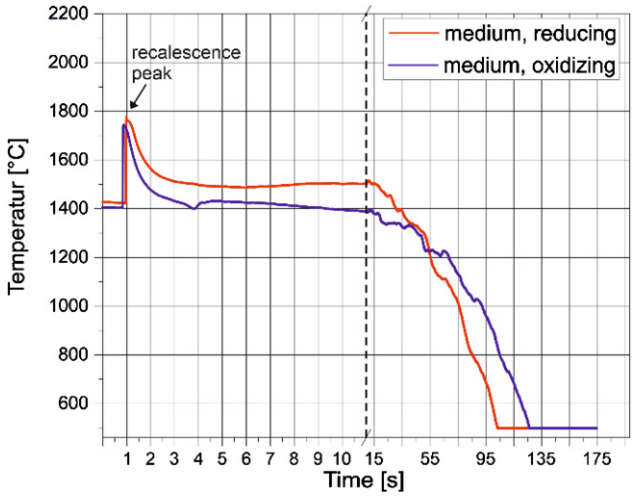

Figure 8. Temperature curves of medium cooled samples from mixture II measured with a pyrometer. The time point 0 was set to 1 s before crystallization.

For detector calibration, CeO_2 powder was encapsulated in a 1 mm diameter Kapton capillary and rolled to a cylinder of about 1 mm diameter. The calibrant was inserted into the levitation nozzle hole thereby centring this reference sample to the sample position. The calibration of the x-ray beam energy and the distance of the detector were refined in an iterative way. Scattering patterns from the calibrant were acquired at five different distances, thus the distance step ΔD_{exact} is a well-known parameter. Using a guess energy, the distance was extracted using the PyFAI-calib2 GUI (Kieffer and Karkoulis 2013), thus $\Delta D_{refined}$ was extracted. The energy is then $\lambda_{refined} = \Delta D_{refined}/\Delta D_{exact} * \lambda_{guess}$. This value was averaged over the five different distances of the detector. The process was repeated until the difference between the guess and refined energies was within the bandwidth of the incident x-ray beam ($\Delta E/E \sim 1 \times 10^{-3}$).

2.4. Data processing

The recorded 2D XRD patterns from the area detector were processed to 1D x-ray diffractograms ($°2\theta_{cu}$ vs intensity) using the pyFAI software (Kieffer and Karkoulis 2013). This approach was chosen to allow comparison with laboratory XRD experiments. The edges of the sample chamber and the shadow of the beamstop were cut off with a mask before processing. The background measurements were also processed with pyFAI and subtracted from the diffractograms before evaluation.

Phase identification was done using the software Match! (Putz 2019) and the crystallographic open database (COD) (Downs and Hall-Wallace 2003, Gražulis *et al* 2009, Gražulis *et al* 2012, Gražulis *et a.* 2015, Merkys *et a.* 2016, Quirós *et al* 2018).

3. Results

3.1. Mixture I (80 mol% CaO + 20 mol% SiO_2)

Mixture I was composed of 80 mol% CaO + 20 mol% SiO_2 and has a melting point around 2300 °C. This temperature could not be achieved with the lasers used in this experiment. The samples only reached a semi-molten state in which some CaO (COD 9006707) continued to be present in crystalline form (figure 3).

Two data sets could be evaluated for this mixture. These included quenching under reducing atmosphere and medium cooling under oxidizing atmosphere. Unfortunately, the latter experiment had to be stopped after only 9 s because the sample stuck to the nozzle before cooling was complete. The cooling rate in the quenching experiment was on average about 300 °C s^{-1}—initially it is faster and becomes gradually slower—corresponding to a cooling time of 6 s from the molten state to room temperature (figure 4).

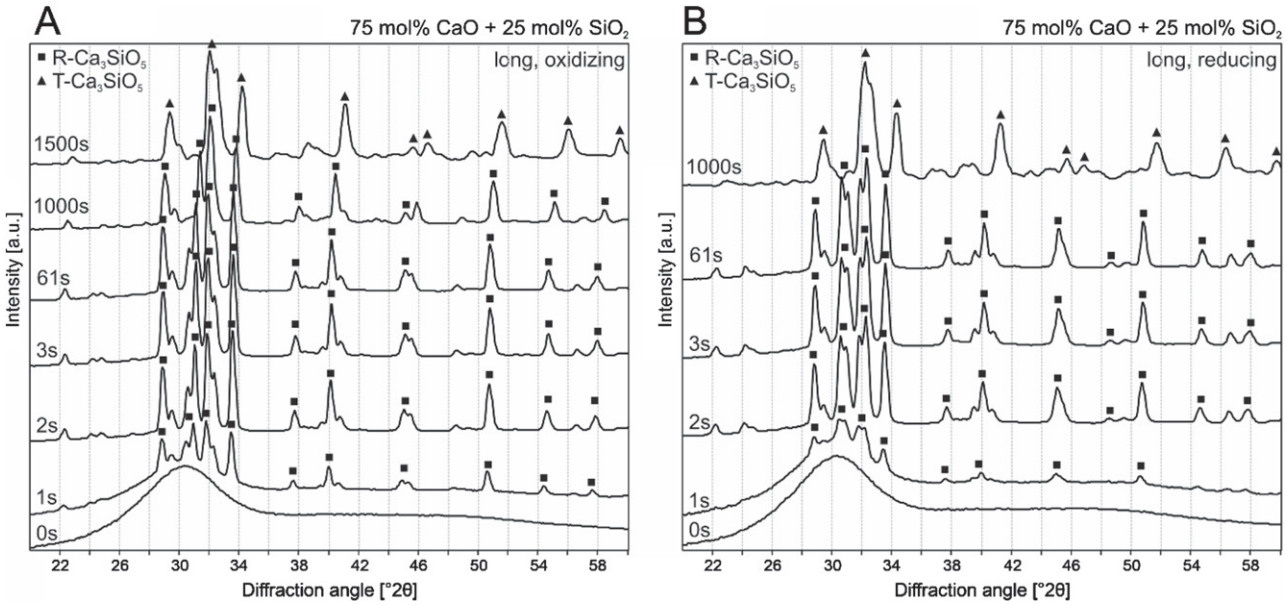

Figure 9. Detail of x-ray diffractograms (20–60 °$2\theta_{Cu}$) of slowly cooled samples from mixture II under (A) oxidizing conditions and (B) reducing conditions. The time point 0 was set to the last diffraction pattern before crystallization.

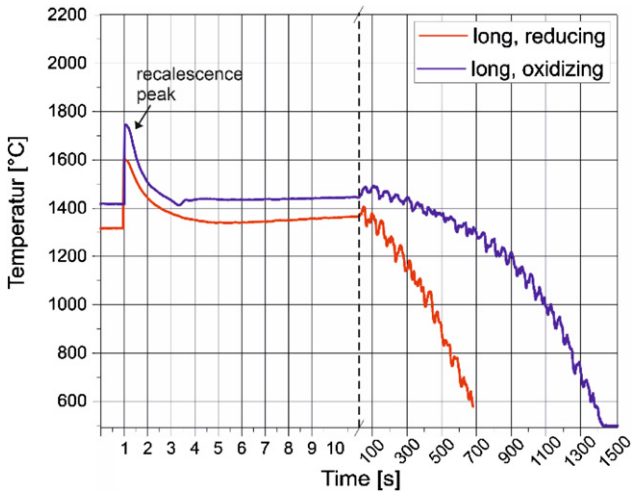

Figure 10. Temperature curves of slowly cooled samples from mixture II measured with a pyrometer. The time point 0 was set to 1 s before crystallization.

Additional to CaO, Ca_3SiO_5 crystallized in both experiments (figure 3) as expected from the phase diagram (figure 1). A modification change of trigonal Ca_3SiO_5 (COD 8104367) to triclinic Ca_3SiO_5 (COD 9014362) was observed in the quenched sample 4 s after the crystallization of Ca_3SiO_5 at a temperature of about 600 °C. The monoclinic modification of Ca_3SiO_5 (COD 9008366) was not observed. However, since the resolution of the diffractograms was too poor to observe the characteristic peak splitting, its diffraction pattern is almost identical to that of the triclinic modification, so that a misinterpretation cannot be excluded.

Since the experiment was stopped before completion, no modification change could be observed in the medium cooled sample. After 9 s of cooling the trigonal modification of Ca_3SiO_5 was still present and the temperature was around 1600 °C.

The medium cooled sample under oxidizing conditions showed a distinct recalescence peak with temperature changes from 1680 to 1750 °C for this single experiment at the moment of Ca_3SiO_5 crystallization (figure 4). The sample processed under reducing atmosphere showed no distinct recalescence peak.

3.2. Mixture II (75 mol% CaO + 25 mol% SiO_2)

For mixture II, experiments could be conducted with all three cooling rates under both reducing and oxidizing conditions. The cooling rates in the quenching experiments averaged about 260 °C s^{-1} under reducing and 180 °C s^{-1} under oxidizing conditions corresponding to a cooling time of 8 s and 7 s, respectively, from the molten state to room temperature (figure 6).

Under oxidizing conditions, trigonal Ca_3SiO_5 (COD 8104367) and CaO crystallized from the melt (figure 5(A)). The time resolution used does not allow to determine the primary solidified phase, since the observations depend on the time of data acquisition relative to the time of solidification.

A modification change of Ca_3SiO_5 to the triclinic modification (COD 9014362) was observed after 6 s corresponding to a temperature around 550 °C. Under reducing conditions, CaO appeared as first crystalline phase followed 2 s later by the trigonal Ca_3SiO_5 (figure 5(B)). 10 s after crystallization, a modification change of Ca_3SiO_5 to the triclinic modification was observed. The sample had already reached room temperature after 7 s (figure 6).

A small recalescence peak occurred in the sample under reducing conditions related to the primary crystallization of

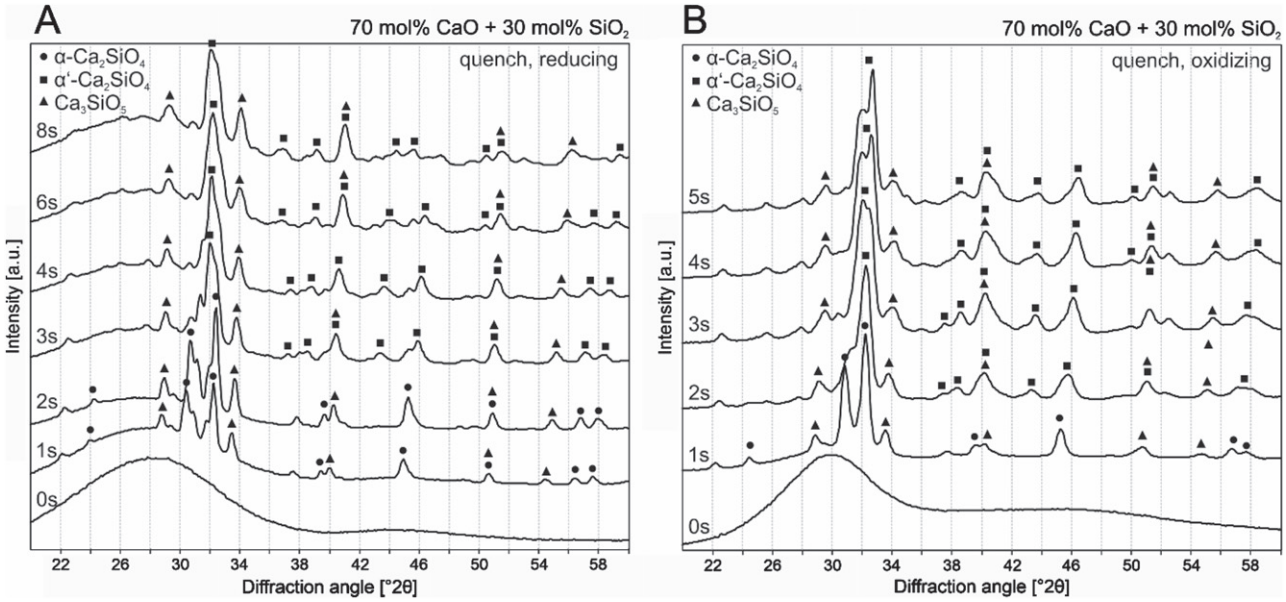

Figure 11. Detail of x-ray diffractograms (20–60 °$2\theta_{Cu}$) of the quenched samples from mixture III. (A) Diffractograms from the first 8 s after quenching under reducing conditions. (B) Diffractograms from the first 5 s after quenching under oxidizing conditions. The time point 0 was set to the last diffraction pattern before Ca_2SiO_4 crystallization.

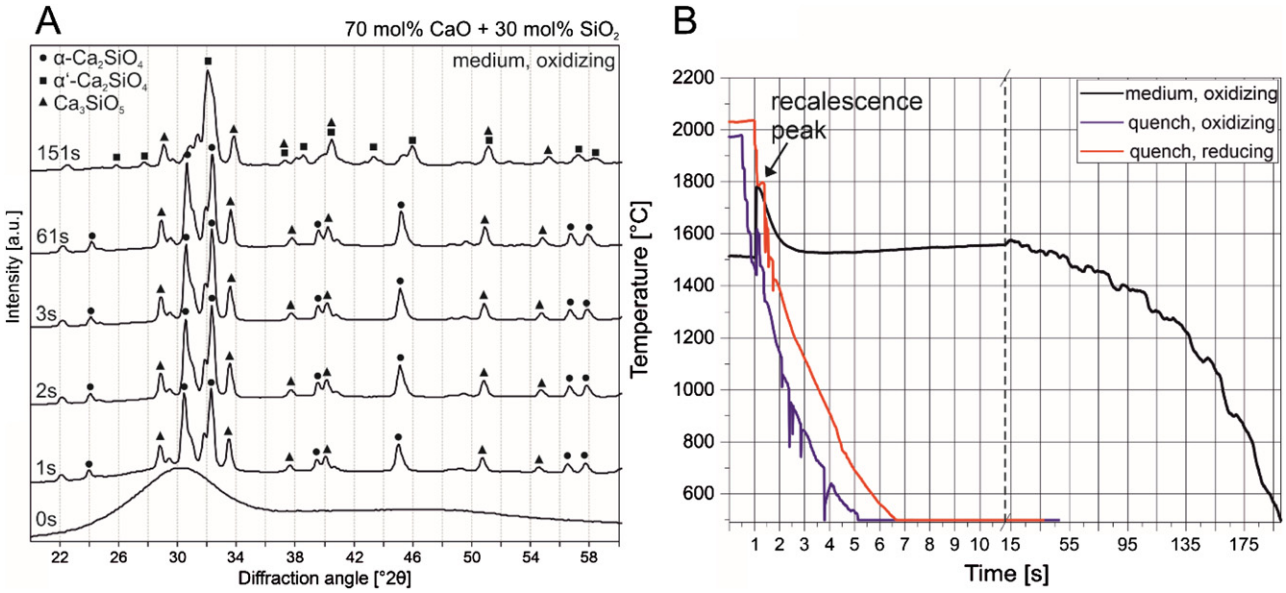

Figure 12. (A) Detail of x-ray diffractograms (20–60 °$2\theta_{Cu}$) from the first 151 s of the medium cooled sample from mixture III under oxidizing conditions. (B) Temperature curves of samples from mixture III during cooling measured with a pyrometer. The time point 0 was set to 1 s before crystallization of Ca_2SiO_4.

CaO (figure 6). No recalescence peak related to the crystallization of Ca_3SiO_5 could be observed in the quenched samples. Therefore, it is possible that the liquid was not or at least not to a large extent undercooled when the crystallization of Ca_3SiO_5 was setting in.

The cooling rates during the medium cooling experiments averaged about 13 °C s^{-1} under reducing and 11 °C s^{-1} under oxidizing conditions corresponding to a cooling time of 105 s and 125 s, respectively, from the molten state to room temperature.

Under both oxidizing and reducing conditions, trigonal Ca_3SiO_5 (COD 8104367) was observed as first crystalline phase (figures 7(A) and (B)). The absence of CaO as primary phase in the medium cooling experiments is probably due to a change in chemical composition during processing, as the samples for the medium cooling experiments were further processed after the quenching experiments. While CaO appeared as a separate phase in the quenching experiments, no CaO peaks were observed in the subsequent medium experiments. This suggests that the CaO content of the samples

decreased during processing. A change in sample mass during the experiments, which was also noticed, supports this observation.

Preferential evaporation of CaO over a period of time that causes a change in sample composition to a more silica-rich melt has been described in the literature (Benmore *et al* 2010). At room temperature, Ca_3SiO_5 was present in the triclinic modification (COD 9014362).

Both medium cooled samples undercooled strongly and showed almost identical recalescence peaks. The temperature change in those experiments was from 1400 to 1750 °C at the moment of crystallization (figure 8). The sharpness of the recalescence peaks indicates that the hypercooling limit may have been exceeded by the sample.

The cooling rates during the long cooling experiments averaged about 1.6 °C s^{-1} under reducing and 1 °C s^{-1} under oxidizing conditions corresponding to a cooling time of 800 s and 1400 s, respectively, from the molten state to room temperature (figure 10).

Comparable to the medium cooled samples, trigonal Ca_3SiO_5 (COD 8104367) crystallized as primary phase under both oxidizing and reducing conditions in the slowly cooled samples (figures 9(A) and (B)). At room temperature, Ca_3SiO_5 was present in the triclinic modification (COD 9014362). Apparently, however, room temperature was reached faster under reducing conditions than under oxidizing conditions (figure 10).

The slowly cooled samples undercooled strongly and showed distinct recalescence peaks. The temperature changes due to recalescence in these experiments were from 1400 to 1750 °C under oxidizing conditions and 1300 to 1600 °C under reducing conditions at the moment of crystallization (figure 10).

3.3. Mixture III (70 mol% CaO + 30 mol% SiO_2)

Mixture III decomposed during cooling due to γ-Ca_2SiO_4 formation. Therefore, repeated heating and cooling cycles were not possible and the experiments had to be stopped as soon as the sample decayed and thus disappeared from the beam. Hence, only single shot experiments could be carried out and only limited data could be recorded for mixture III.

All in all, the data of three experiments could be evaluated. These experiments included quenching under oxidizing and reducing conditions and medium cooling under oxidizing conditions. The cooling rates in the quenching experiments averaged about 300 °C s^{-1} under reducing and 400 °C s^{-1} under oxidizing conditions corresponding to a cooling time of 7 s and 5 s, respectively, from the molten state to room temperature. The cooling rate during the medium cooling experiment averaged about 8 °C s^{-1} corresponding to a cooling time of 200 s from the molten state to room temperature.

The crystallization of α-Ca_2SiO_4 (COD 1546028) and Ca_3SiO_5 could be observed in all three experiments, as expected from the phase diagram (figure 1). Due to the strong overlap with the α-Ca_2SiO_4 peaks, the Ca_3SiO_5 modification could not be determined.

A modification change from α-Ca_2SiO_4 to α'-Ca_2SiO_4 was observed after 2–3 s in the quenched samples and after 150 s in the medium cooled sample corresponding to a temperature around 1100 °C in both cases (figures 11 and 12). It was not possible to distinguish between α'_H (COD 1546027) and α'_L (COD 1546026) modification due to their similar XRD patterns. According to literature, the α to α'-modification change occurs at 1425 °C (Chan *et al* 1992). The discrepancy to the temperature observed here is due to the fact that the temperature given is for equilibrium conditions which were not achieved in this experiment.

The melting point of Ca_2SiO_4 is 2150 °C. However, the samples processed under oxidizing conditions undercooled strongly and showed distinct recalescence peaks with temperature changes from 1450 to 1600 °C in the quenched sample and from 1500 to 1800 °C in the medium cooled sample at the moment of crystallization in the respective experiments (figure 12). The sample processed under reducing atmosphere showed no distinct recalescence peak.

4. Discussion

The differentiation of Ca_3SiO_5 polymorphs with XRD is not straightforward since the differences between the diffraction patterns of the individual modifications are small (Bigare *et al* 1967, Dunstetter *et al* 2006). Mainly the peaks in the angular range 31.5 to 32.5 °$2\theta_{Cu}$ and 51 to 52 °$2\theta_{Cu}$ are suited for a differentiation. In this range, the peaks of the rhombohedral pattern change during cooling due to small deformations of the rhombohedral unit cell (Bigare *et al* 1967). However, the resolution of the recorded diffractograms was too low to resolve the characteristic peak splitting. The pixel size of the detector used was relatively large and the radial integration of the acquired 2D diffraction pattern further reduced the resolution. The resolution decreases with increasing angle since the detector is flat and the active area of the pixels has a non-negligible thickness. For this reason, the resolution of the range 51–52 °$2\theta_{Cu}$ was worse than that of the range 31.5–32.5 °$2\theta_{Cu}$ range, and only the latter range was evaluated. To improve the resolution, the experimental set-up would have to be adjusted, for example with a point detector or a larger detector-sample distances.

The polymorphs were distinguished by comparison with reference diffractograms. This worked well for distinguishing the trigonal and triclinic polymorphs but was difficult for distinguishing the monoclinic and triclinic polymorphs.

The data from these experiments were compared to the trigonal modification R determined by Nishi and Takéuchi (1984) (COD 8104367), the monoclinic M3 modification determined by Nishi *et al* (1985) (COD 9008366) and the triclinic modifications T3 and T1 described by De La Torre *et al* (2008) (COD 9016125) and Golovastikov *et al* (1975) (COD 9014362), respectively (figure 13). No reference data were available for the M1, M2 and T2 polymorphs, since, to our knowledge, no structure of M2 is described in the literature and the data for both the T2 polymorph determined by Peterson *et al* (2004) and the M1 polymorph determined by De Noirfontaine *et al* (2012) are not available in the COD. The reference data for

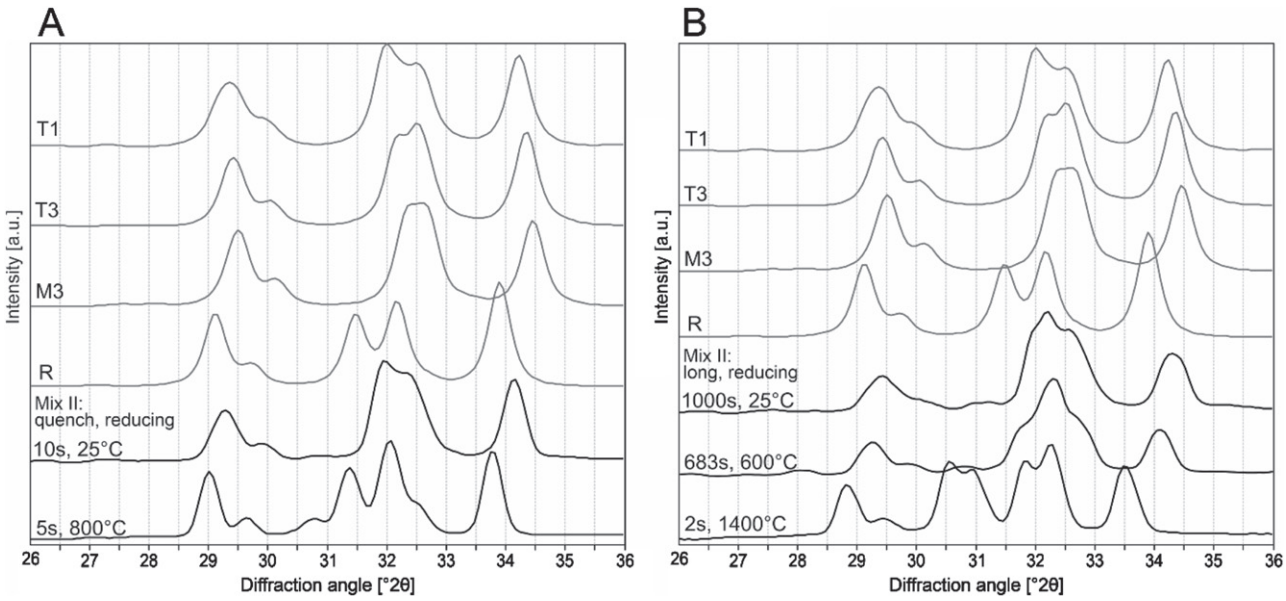

Figure 13. Comparison of the angular region 26–36 °$2\theta_{Cu}$ of the reference R (Nishi and Takéuchi 1984) (COD 8104367), M3 (Nishi *et al* 1985) (COD 9008366), T3 (De La Torre *et al* 2008) (COD 9016125) and T1 (Golovastikov *et al* 1975) (COD 9014362) with (A) a sample of mixture II quenched under reducing conditions and (B) a sample of mixture II slowly cooled (1.6 °C s^{-1}) under reducing conditions at high temperatures and at room temperature. The specified times refer to the time elapsed after the last recorded diffractogram in the molten state.

α, α'_H- and α'_L-Ca_2SiO_4 were COD 1546026 to 1546028 determined by Mumme *et al* (1996).

No monoclinic modification was observed in the quenched sample of mixture II. The trigonal high-temperature polymorph was still detected at a temperature of 800 °C, at which the monoclinic polymorphs are already stable (980–1070 °C). The reason for this could be either that the quenched sample changes directly from the trigonal to the triclinic structure due to the high cooling rate or that the change is too fast to be detected with the currently used recording speed of 1 diffractogram per second. At room temperature, the stable T1 polymorph was found as expected.

At 1400 °C, the peak shape of the slowly cooled sample differs from the trigonal reference pattern. This may be due to the fact, that the reference pattern was recorded using a tricalcium silicate solid solution with Al quenched from 1200 °C. The monoclinic polymorph was observed at about 600 °C outside the described stable temperature range. This is again due to the non-equilibrium conditions in the experiment. The diffraction pattern also differed slightly from the M3 reference pattern, presumably because these were not determined on pure tricalcium silicate. Again, the expected T1 polymorph was found at room temperature.

Recalescence refers to the release of latent heat of crystallization that causes a sudden increase of temperature of the sample. The quenched and medium cooled samples of mixture III as well as the medium cooled sample of mixture I processed under oxidizing conditions showed distinct recalescence. In mixture II, recalescence was observed in all medium and slowly cooled samples independent of atmospheric conditions and at almost identical temperature. No recalescence was observed in the quenched samples of mixture I and III under reducing conditions and of mixture II under both reducing and oxidizing conditions.

Undercooling is common in levitated samples since heterogeneous nucleation by contact with the crucible is suppressed and the nucleation rate of the crystals in melt is considerably reduced. The amount of undercooling of the samples was between 550 and 770 °C. It is to be evaluated whether the hypercooling limit was indeed exceeded, as indicated by the rather sharp recalescence peaks without a solidification plateau as part of the recalescence peak, and the recalescence temperatures not conforming to any of the known temperatures in the phase diagram.

The samples of mixture II processed under reducing conditions reached room temperature faster than the ones processed under oxidizing conditions beside identical laser power ramp. The opposite was observed for the quenched samples of mixture III. Here the samples cooled faster under oxidizing conditions. This behaviour might have different origins that cannot be conclusively answered at present. It could be that indeed the reported differences are real. However, it could equally be that the surface of the sample is modified by switching from reducing to oxidizing conditions. As a result, emissivity might change. In addition, emissivity might change upon crystallization and might continue to do this during further cooling.

No signs for Ca_3SiO_5 decomposition were observed in the experiments. This is consistent with the literature since according to Tenório *et al* (2007) a cooling rate of 0.5 °C min^{-1} (0.008 °C s^{-1}) is required for a complete decomposition. For a cooling rate of 10 °C min^{-1} (0.16 °C s^{-1}) less than 20 % decomposition of Ca_3SiO_5 was observed (Tenório *et al* 2007). In this experiment, the slowest average cooling rate was

60°C min^{-1} (1 °C s^{-1}). Therefore, cooling was too rapid to induce a decomposition of Ca_3SiO_5 as observed under equilibrium conditions.

In mixture II, CaO was observed as a single phase in the first experiments but disappeared in subsequent experiments on the same sample. Furthermore, since the samples suffered a significant weight loss during the experiments, a change in chemical composition towards a more Si-rich composition is likely and consistent with the literature (Benmore *et al* 2010). However, since Ca_3SiO_5 continued to be the major phase in the CaO-depleted samples, we assume that the altered composition is not so far from the intended composition as to invalidate the interpretation.

Whether there is a complete absence of Ca_2SiO_4 formation in mixture II during cooling is to be further looked into. One reason might be that the hypercooling limit is reached.

5. Conclusions

In this study, the crystallization and phase evolution of samples in the compositional range between 70–80 mol% CaO and 30–20 mol% SiO_2 was investigated during cooling at different rates under reducing and oxidizing conditions.

Although not all investigated mixtures could be processed under all conditions, it was possible to observe crystallization of primary phases according to the phase diagram in all mixtures despite their sometimes deep undercoolings which would open up pathways for metastable phase formation. Moreover, the modification changes of di- and tricalcium silicate could be observed *in situ*.

The average cooling rates applied were 200–300 °C s^{-1} (quench), 11–13 °C s^{-1} (medium cooled) and 1–2 °C s^{-1} (slowly cooled). These cooling rates are too high for thermodynamic equilibrium to occur. Thus, no decomposition of tricalcium silicate was observed and the modification changes occurred at lower temperatures than under equilibrium conditions. All samples severely undercooled and most showed recalescence.

The reducing atmosphere was generated using Ar as levitation gas, and the oxidizing atmosphere was generated using a mixture of Ar and O_2 as levitation gas. No changes in phase evolution were observed under different atmospheric conditions.

The combination of ADL with synchrotron XRD allows *in situ* observation of the phase evolution of mixtures with high melting points from melt to room temperature. The setup holds numerous possibilities for all types of high-temperature research due to crucible-free processing and variability of cooling rates and atmospheric conditions.

It could even be used to study the polymorphs of pure tricalcium silicate in a wider temperature range. For this, however, the samples would have to be kept at certain temperatures for some time to achieve the stable modification at that temperature. In addition, some adjustments to the XRD system may be necessary for this purpose. Further, the use of a faster detector or recording speed might be considered for the observed sub-second primary phase formation.

CRediT author statement

Katharina Schraut: conceptualization, investigation, writing—original draft.

Florian Kargl: conceptualization, methodology, investigation, writing—review & editing, funding acquisition.

Christian Adam: conceptualization, investigation, writing—review & editing, funding acquisition.

Oleh Ivashko: investigation, methodology, writing—review & editing.

This work was funded by Bundesanstalt für Materialforschung und -prüfung (BAM) and Deutsches Zentrum für Luft und Raumfahrt (DLR).

Acknowledgments

We acknowledge DESY (Hamburg, Germany), a member of the Helmholtz Association HGF, for the provision of experimental facilities. This research was carried out at PETRA III and we would like to thank Ann-Christin Dippel, Martin von Zimmermann, Philipp Glaevecke, Olof Gutowski and Soham Banerjee for their assistance at Beamline P21.1.

Data availability statement

The data that support the findings of this study are available upon reasonable request from the authors.

ORCID iDs

Katharina Schraut https://orcid.org/0000-0002-2740-1539
Florian Kargl https://orcid.org/0000-0001-9902-0420
Christian Adam https://orcid.org/0000-0002-3356-4617
Oleh Ivashko https://orcid.org/0000-0002-4869-8175

References

Bazzoni A, Ma S, Wang Q, Shen X, Cantoni M and Scrivener K L 2014 *J. Am. Ceram. Soc.* **97** 3684–93
Benmore C J, Weber J, Wilding M C, Du J and Parise J B 2010 *Phys. Rev.* B **82** 224202
Bigare M, Guinier A, Mazieres C, Regourd M, Yannaquis N, Eysbl W, Hahn T and Woermann E 1967 *J. Am. Ceram. Soc.* **50** 609–19
Carlson E T 1931 *Bur. Stand. J. Res.* **7** 893–902
Chan C J, Kriven W M and Young J F 1992 *J. Am. Ceram. Soc.* **75** 1621–7
Day A L and Shepherd E S 1906 *J. Am. Chem. Soc.* **28** 1089–114
De La Torre Á G, Bruque S, Campo J and Aranda M A G 2002 *Cem. Concr. Res.* **32** 1347–56
De la Torre Á G, De Vera R N, Cuberos A J M and Aranda M A G 2008 *Cem. Concr. Res.* **38** 1261–9
De Noirfontaine M-N, Courtial M, Dunstetter F, Gasecki G and Signes-Frehel M 2012 *Z. Kristallogr.* **227** 102–12
Downs R T and Hall-Wallace M 2003 *Am. Mineral.* **88** 247–50
Dunstetter F, De Noirfontaine M-N and Courtial M 2006 *Cem. Concr. Res.* **36** 39–53
Durinck D, Engström F, Arnout S, Heulens J, Jones P T, Björkman B, Blanpain B and Wollants P 2008 *Resour., Conserv. Recycl.* **52** 1121–31
Ghosh S N, Rao P B, Paul A K and Raina K 1979 *J. Mater. Sci.* **14** 1554–66

Glasser F P 1998 The burning of Portland cement *Lea's Chemistry of Cement and Concrete* ed P Hewlett (London: Arnold) pp 195–240
Golovastikov N, Matveeva R and Belov N 1975 *Sov. Phys. Crystallogr.* **20** 441–5
Gražulis S *et al* 2009 *J. Appl. Crystallogr.* **42** 726–9
Gražulis S *et al* 2012 *Nucl. Acids Res.* **40** D420–7
Gražulis S, Merkys A, Vaitkus A and Okulič-Kazarinas M 2015 *J. Appl. Crystallogr.* **48** 85–91
Jeffery J W 1952 *Acta Crystallogr.* **5** 26–35
Kargl F, Yuan C and Greaves G N 2015 *Int. J. Microgravity Sci. Appl.* **32** 320200
Kieffer J and Karkoulis D 2013 PyFAI, a versatile library for azimuthal regrouping *J. Phys.: Conf. Ser.* **425** 202012
Kühl H 1951 *Zement-Chemie: Das Wesen und die Herstellung der hydraulischen Bindemittel* (Berlin: Verlag Technik)
Lea F M and Parker T W 1934 *Phil. Trans. R. Soc.* **234** 1–41
Li X, Shen X, Tang M and Li X 2014 *Ind. Eng. Chem. Res.* **53** 1954–64
Ludwig H-M and Zhang W 2015 *Cem. Concr. Res.* **78** 24–37
Macphee D E and Lachowski E E 2003 Cement components and their phase relations *Lea's Chemistry of Cement and Concrete* ed P Hewlett (London: Arnold) pp 95–129
Maki I, Fukuda K, Seki S and Tanioka T 1991 *J. Am. Ceram. Soc.* **74** 2082–5
Merkys A, Vaitkus A, Butkus J, Okulič-Kazarinas M, Kairys V and Gražulis S 2016 *J. Appl. Crystallogr.* **49** 292–301
Mohan K and Glasser F 1977 *Cem. Concr. Res.* **7** 1–7
Mumme W, Cranswick L and Chakoumakos B 1996 *J. Solid State Chem.* **172** 178–87
Nishi F and Takéuchi Y 1984 *Z. Kristallogr.* **168** 197–212
Nishi F, Takéuchi Y and Iwao I 1985 *Z. Kristallogr.* **172** 297–314
Nurse R 1960 Phase equilibria and constitution of Portland cement clinker *4th Int. Symp. on the Chemistry of Cement*
Peterson V K, Hunter B A and Ray A 2004 *J. Am. Ceram. Soc.* **87** 1625–34
Putz H 2019 *Match! 3 3.8.0.137*
Quirós M, Gražulis S, Girdzijauskaitė S, Merkys A and Vaitkus A 2018 *J. Cheminf.* **10** 1–17
Rankin G A 1915 *Am. J. Sci.* **1** 79
Sinclair W and Groves G W 1984 *J. Am. Ceram. Soc.* **67** 325–30
Stephan D 1999 Chrom, Nickel und Zink in Klinker und Zement: Einbau, Eigenschaftsänderung und Auslaugung *PhD Thesis* Universität-Gesamthochschule Siegen
Taylor H F 1997 *Cement Chemistry* (London: Thomas Telford)
Tenório J A S, Pereira S S R, Barros A M, Ferreira A V, Espinosa D C R and Araújo F G S 2007 *Mater. Res. Bull.* **42** 1099–103
Woermann E 1960 Decomposition of alite in technical Portland cement clinker *4th Int. Symp. in the Chemistry of Cement*
Yamaguchi G and Miyabe H 1960 *J. Am. Ceram. Soc.* **43** 219–23
Yannaquis N, Regourd M, Mazières C and Guinier A 1962 *BULMI* **85** 271–81